A physico-chemical investigation of highly concentrated potassium acetate solutions towards applications in electrochemistry

*Pierre L. Stigliano [a], Nicolò Pianta [a], Simone Bonizzoni [a], Michele Mauri [a], Roberto Simonutti [a], Roberto Lorenzi [a], Barbara Vigani [b], Vittorio Berbenni [c], Silvia Rossi [b], Piercarlo Mustarelli [ad] and Riccardo Ruffo *[ad]*

[a]*Department of Materials Science, University of Milan-Bicocca, Via Cozzi 55, Milano, 20125, Italy*
[b]*Department of Drug Sciences, University of Pavia, Viale Taramelli 12, 27100 Pavia, Italy*
[c]*Department of Chemistry, University of Pavia, Viale Taramelli 16, 27100 Pavia, Italy*
[d]*National Reference Center for Electrochemical Energy Storage (GISEL) – INSTM, Via G. Giusti 9, 50121 Firenze, Italy*

**Corresponding author: riccardo.ruffo@unimib.it*

Abstract

Water-in-salt solutions, *i.e.* solutions in which the amount of salt by volume or weight is larger than that of the solvent, are attracting increasing attention in electrochemistry due to their distinct features that often include decomposition potentials much higher than those of lower concentration solutions. Despite the high solubility of potassium acetate (KAC) in water at room temperature (up to 25 moles of salt per kg of solvent), the low cost, and the large availability, the use of highly concentrated KAC solutions is still limited to a few examples in energy storage applications and a systematic study of their physical–chemical properties is lacking. To fill this gap, we have investigated the thermal, rheological, electrical, electrochemical, and spectroscopic features of KAC/water solutions in the compositional range between 1 and 25 mol kg^{-1}. We show the presence of a transition between the "salt-in-solvent" and "solvent-in-salt" regimes in the range of 10–15 mol kg^{-1}. Among the explored compositions, the highest concentrations (20 and 25 mol kg^{-1}) exhibit good room temperature conductivity values (55.6 and 31 mS cm^{-1}, respectively) and a large electrochemical potential window (above 2.5 V).

Introduction

The properties of electrolyte solutions are strongly influenced by the salt concentration, and the electrolyte composition must be carefully designed to optimize the performances of electrochemical devices.[1–3] To minimize the voltage drop in galvanic cells, usually, the optimal composition of the electrolyte lies around the maximum of the conductivity *vs.* concentration curve, *i.e.* where the ion amount is high enough to provide a large number of charge carriers, without depressing their mobility due to viscosity issues. At the same time, it is mandatory to avoid the onset of strong interactions among the solution components, leading to salt reassociation (*e.g.* formation of ion-pairs and triplets). Thus, in aqueous electrolytes, optimized concentrations lie usually in the range of 5–10 m, while for organic-based electrolytes (*e.g.* for lithium-ion batteries, LIBs) the optimal values are in the (lower) range of 0.1–2 M, due to the different dielectric properties of the solvents.[4] However, the salt concentration also plays a relevant role on the electrochemical properties of the solution, *e.g.* the potential stability range, and/or the kinetic parameters of the electrochemical reactions, *e.g.* exchange current densities. Thus, in recent years, a renewed and growing interest in the development of highly concentrated electrolytes for energy storage has appeared in the literature which has led to a new definition of the concentration fields in terms of volume or weight ratio: the "solvent-in-salt" systems,[5] a term derived from a pioneering paper on polymer electrolytes.[6] Whereas most of these works have been devoted to the development of organic electrolytes, such as LiTFSI in mixtures of 1,3-dioxolane (DOL) and dimethoxyethane (DME), the same concept has also been applied to aqueous solutions, declining it as "water-in-salt".[7] Here, the main aim is to extend the electrochemical stability window of H_2O beyond its thermodynamic limit by playing with its activity coefficient, and it has been demonstrated that using a 21 m solution of LiTFSI in water it is possible to span 3.0 V without any solvent decomposition. The resulting electrolyte has been applied in lithium ion batteries (LIBs); however, the price of the salt (in the range of 30–200 \$ kg^{-1}) practically nullifies one of the main advantages of aqueous electrolytes, namely their low cost. In contrast, there are examples of highly soluble, largely available and cheap salts which can be used in energy storage devices. Among them, two examples are LiCl and CH_3COOK, which have been used in hybrid and symmetric supercapacitors at concentrations of 20 and 7.8 mol kg^{-1}, respectively.[8,9]

Potassium acetate (KAC) is quite interesting in this framework, also due to its applicability in potassium-ion batteries,[10] as well as in mixed electrolytes for lithium-ion systems.[11] KAC solubility at RT is about 2700 g l^{-1} and solutions with a molality larger than 20 m can be prepared. At this

concentration, the KAC/water solution shows a conductivity of 50 mS cm^{-1}, *i.e.* 5 times larger than that of LiTFSI.[10] Although applications of the KAC/water systems have already been reported in the literature, a systematic investigation of these electrolyte solutions is still missing. The aim of this work is to obtain a detailed insight into the physical chemistry of KAC solutions in the concentration range from 1 m to 25 m. We have thus investigated the rheological, thermal, electrical, and electrochemical properties. We have also tried to correlate the physico-chemical bulk properties with the solvent–salt interactions by means of Raman spectroscopy.

Experimental section

Six different solutions were prepared using CH_3COOK (Alfa Aesar, 99%) and H_2O Milli-Q® (Millipore) according to their molality, ranging from 1 to 25 (see Table 1). In the following, the samples will be named KAC-*n* (*n* = molality). The highest value was chosen close to the salt solubility limit at 25 °C,[12] which corresponds to a molality of 27.4 mol kg^{-1}. In this concentration range, a solution with a molality higher than 10 mol kg^{-1} can be considered as a solvent-in-salt system by weight. The density of the solutions was measured using both volumetric and gravimetric methods and the values were used to recalculate the molarities, which are needed to obtain the molar conductivity. Table 1 reports full information on the stoichiometry of the solutions.

Sample name	Molality(*m*) (mol_{KAC} kg_{H2O}^{-1})	Density (g cm^{-3})	Molarity (mol_{KAC} dm^{-3})	Mol KAC (%)	Mol H_2O (%)	Wt KAC (%)	Wt H_2O (%)	*n**
KAC-1	1	1.03	0.94	1.8	98.2	8.9	91.1	55.55
KAC-5	5	1.18	3.94	8.3	91.7	32.9	67.1	11.11
KAC-10	10	1.29	6.51	15.3	84.7	49.5	50.5	5.55
KAC-15	15	1.33	8.08	21.3	78.7	59.6	40.4	3.70
KAC-20	20	1.36	9.18	26.5	73.5	66.3	33.7	2.70
KAC-25	25	1.38	10.00	31.1	68.9	71.0	29.0	2.22

*n** = number of water molecules/number of KAC molecules.

Table 1 *Composition parameters of the KAC–H_2O solutions*

Thermal analysis

Differential Scanning Calorimetry (DSC) measurements were carried out on ∼ 20 mg of KAC aqueous solutions in Al crucibles using a DSC 1 Star® System (Mettler Toledo), and the data were evaluated using STARe® Software. The samples were tested in the temperature range from −120 °C to 20 °C with the following protocol: 5 min at −120 °C, from −120 °C to 20 °C at 5 °C min^{-1}, 5 min at 20 °C, from 20 °C to −120 °C at 1 °C min^{-1}, 5 min at −120 °C, from −120 °C to 20 °C at 5 °C min^{-1}. The ramp from 20 °C to −120 °C at 1 °C min^{-1} was performed in order to allow the systems to undergo structural relaxation and, possibly, full crystallization. The relevant temperatures were measured during the final heating ramp.

Viscosity

Viscosity measurements were performed on an MCR 102 rheometer (Anton Paar). Shear tests were carried out using a parallel plate (50 mm) setup with shear rates from 10 to 300 s^{-1} and 100 s for stabilization. Four values of temperature were measured: 20 °C, 50 °C, 60 °C, and 70 °C.

Ionic conductivity

Ionic conductivity was measured *via* Electrochemical Impedance Spectroscopy (EIS) using a dip cell probe consisting of two platinum foils sheathed in glass, with a cell factor of 0.97 cm^{-1}. Impedance spectra were measured over the frequency range of 1 MHz–100 mHz with a 10 mV amplitude. The analysis was conducted under N_2 flux from 5 °C to 75 °C with 5 °C steps in a climatic chamber (Angelantoni, Italy). The bulk ohmic resistance was determined from the high frequency intercept in the Nyquist plot of the impedance data.

Electrochemical characterization

Linear sweep voltammetry (LSV) experiments to evaluate the electrochemical stability window were performed on three-electrode flooded cells equipped with a glassy carbon working electrode, a Pt foil counter electrode and a saturated calomelane reference electrode (+0.244 V *vs.* SHE). The potential range was from −1.500 V (−1.249 V *vs.* SHE) to 1.500 V (1.741 *vs.* SHE) with a scan rate of 1 mV s^{-1}. Current densities of 0.1 mA cm^{-2} are considered as thresholds for the estimation of decomposition potentials.

Raman spectroscopy

Micro-Raman measurements were carried out at room temperature using a confocal LabRAM (Horiba Jobin-Yvon) spectrometer, operating in backscattering configuration. An Ar^+ laser line at 488 nm was used as the excitation source with a spectral resolution of 2 cm^{-1}. The scattered light was detected using a charge coupled device (CCD-Sincerity, Jobin Yvon). A microscope (Olympus BX40) was used to focus the excitation on the samples and to collect the scattered radiation using a Long Working Distance 50x objective with a numerical aperture of 0.60 and a laser power on the sample of <1 mW. The Raman spectra of acetate solutions were acquired through glass vials and the samples were kept sealed during spectrum collection.

Results and discussion

Fig. 1 shows the DSC thermograms of the KAC solutions (a) and a tentative phase diagram sketched on the basis of the thermal data (b). The DSC curves show three relevant thermal features, some of which were observed only for some samples, namely, the glass transition temperature, T_g, the cold crystallization exotherm, T_c, and one or two melting endotherms, T_m.

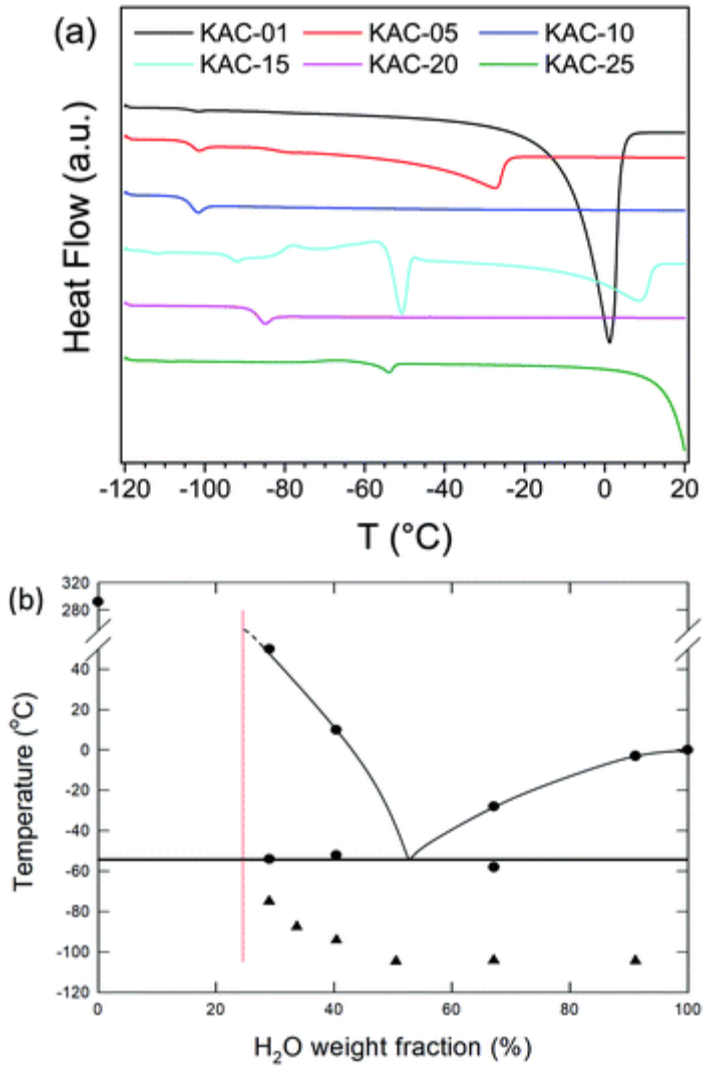

Fig. 1 *(a) DSC thermograms of the KAC solutions. The molality increases from top to bottom; (b) tentative phase diagram of the KAC-H_2O system. Full triangles indicate the glass transition temperatures, T_g, measured via DSC. The red dashed line represents the room temperature solubility limit.*[7]

Regarding the evolution of T_g with salt concentration, we noticed that the values are nearly constant up to KAC-10 and then increase with molality (see Fig. 1b), which reflects a growing interaction between the ions inside the solution above this concentration (see also the Raman results). On the other hand, the concentration zone between KAC-10 and KAC-15 sets the actual transition from the salt-in-solvent to the solvent-in-salt region, and a similar T_g increase was also observed for LiTFSI in DOL/DME.[5] From Table 1, this corresponds to about 4–5 H_2O molecules per K^+ ion. This point will be further discussed in the following. Noteworthily, the glass transitions generally ended with an endothermic feature (overshoot) that can be related to structural relaxation.[13] Cold crystallization exotherms may be observed for KAC-15 and, to a lesser extent, for

samples KAC-5 and KAC-25. Interestingly, KAC-10 and KAC-20 did not show any exotherm above the glass transition, which means a higher resistance towards crystallization. While the thermal behaviour is dependent on the heating rate, since all the samples were subjected to the same thermal history, the behaviour of sample KAC-15 is anomalous and suggests greater ease in the formation of crystalline complexes.

Finally, single melting endotherms were observed for KAC-1 and KAC-5, whereas KAC-15 and KAC-25 showed two peaks, which can be attributed to the eutectic arrest (around −55 °C) and to the liquidus point, respectively. On this basis, the tentative phase diagram of the KAC–H_2O systems can be sketched as shown in Fig. 1b. Our tentative phase diagram is in good agreement with previously reported data.[14,15] In the case of KAC-1, the eutectic arrest is likely too small to be observed, whereas the endotherm of KAC-5 starts very close to the arrest temperature, suggesting that this last one is not observed due to the dynamic nature of the DSC measurement. Although theorrectl series of the thermograms points towards the orrectess of the phase diagram, we recognize that some parts of it are the result of inferences, which take into account the dynamic nature of the DSC experiment.

Fig. 2 shows the Arrhenius plot of viscosity *vs.* reciprocal temperature. The viscosity data are in agreement with those already reported for concentrations lower than 15 m.[16] All the samples behave like Newtonian fluids, as shown by the flow curves presented in the ESI† (Fig. S1–S6), except for KAC-1 which shows a slight plastic behaviour above 50 °C, probably due to measurement inaccuracies, as the viscosity is close to the lower sensitivity limit of the instrument. The data could be fitted with the semi-empirical Vogel–Tammann–Fulcher equation (see for example ref. 17).

$$\eta = \eta_0 \exp\left(\frac{B}{T - T_0}\right) \quad (1)$$

where B is the pseudo-activation energy expressed in Kelvin and T_0 is a parameter which may be related to an “ideal” glass transition temperature. However, due to the limited temperature range explored in this work, the viscosity data are well fitted with the simpler Arrhenius equation:

$$\eta = \eta_0 \exp\left(\frac{E_a}{RT}\right) \quad (2)$$

where E_a is the activation energy related to ion–ion bulk interactions and R is the gas constant. The E_a values are reported in Table 2. The activation energy is nearly constant up to 10 m and then rapidly increases with the solution concentration, in agreement with the behaviour of the glass transition temperature. Interestingly, if we consider an average solvent coordination number of 45 for the K ions (see also the Raman results) a steep increase of E_a occurs when all the water molecules interact with the salt cations.

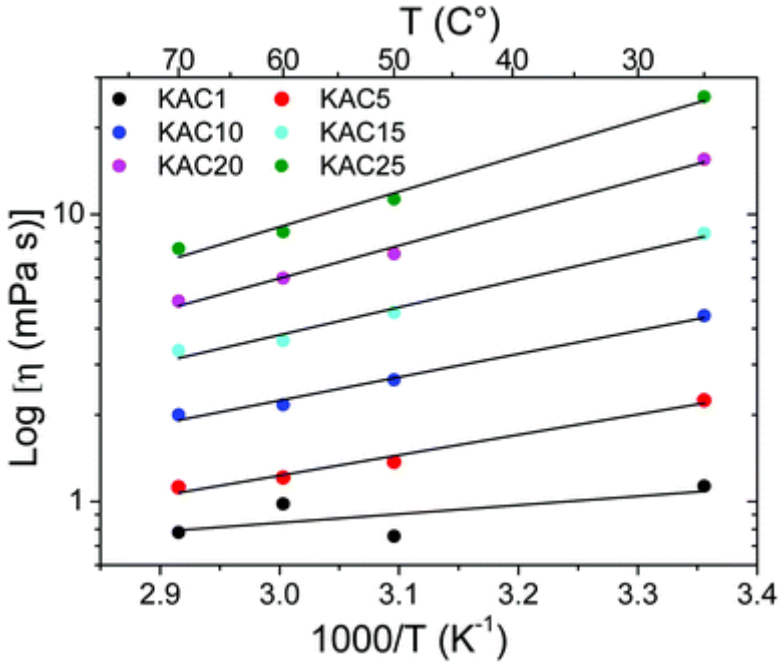

Fig. 2 *Arrhenius plot of viscosity (η). The lines indicate linear regressions (R^2 > 98%, but for KAC-1, see the text). Errors are given inside the symbol dimensions. Full data with standard deviations are reported in Fig. S1–S6 (ESI†).*

Sample name	Molality (mol kg^{-1})	ln η_0 (mPa s)	$E_a(\eta)$ (eV)	σ (25 °C) (mS cm^{-1})	Λ_m (25 °C) (S cm^2 mol^{-1})	ln σ_0 (S cm^{-1})	$E_a(\sigma)$ (eV)	T_0 (K)
KAC-1	1	–9.2	0.06	60.8	64.9	0.06	0.04	143
KAC-5	5	–5.0	0.06	128	32.4	0.21	0.02	178
KAC-10	10	–5.1	0.07	111	17.0	0.20	0.05	195
KAC-15	15	–12.0	0.19	80.5	9.96	0.26	0.08	196
KAC-20	20	–12.9	0.23	55.6	6.06	0.22	0.13	201
KAC-25	25	–13.3	0.25	31.0	3.10	0.23	0.17	204

Table 2 *Experimental conductivity values and best-fit parameters of viscosity and conductivity data(σ = specific conductivity; Λ_m = molar conductivity; ln η_0 = Arrhenius prefactor from*

viscosity; $E_a(\eta)$ = Arrhenius activation energy from viscosity; ln σ_0 = VTF prefactor from conductivity; $E_a(\sigma)$ = VTF activation energy from conductivity; T_0 = VTF temperature parameter.)

Fig. 3 shows how the ionic conductivity depends on the temperature for concentration isopleths (a) and its behaviour *vs.* solution concentration at different temperatures (b). The observed values are in good agreement with the results recently reported by Wu *et al.*[18] Considering the KAC solubility limit *vs.* temperature,[12] the 25 m solution is supersaturated below ~13 °C; however, we did not observe any salt precipitation during the measurements. The Arrhenius-like diagram in Fig. 3a allows the appreciation of the goodness of fits obtained using the VTF equation:

$$\sigma = \sigma_0 \exp\left(\frac{-B'}{T - T_0}\right) \quad (3)$$

where B' and T_0 have the same meaning discussed for eqn (1). The best-fit gives an activation energy of 0.04 eV, in good agreement with the activation energy from viscosity (see Table 2). Table 2 reports the best-fit parameters and the molar conductivity, Λ_m, values obtained at 25 °C.

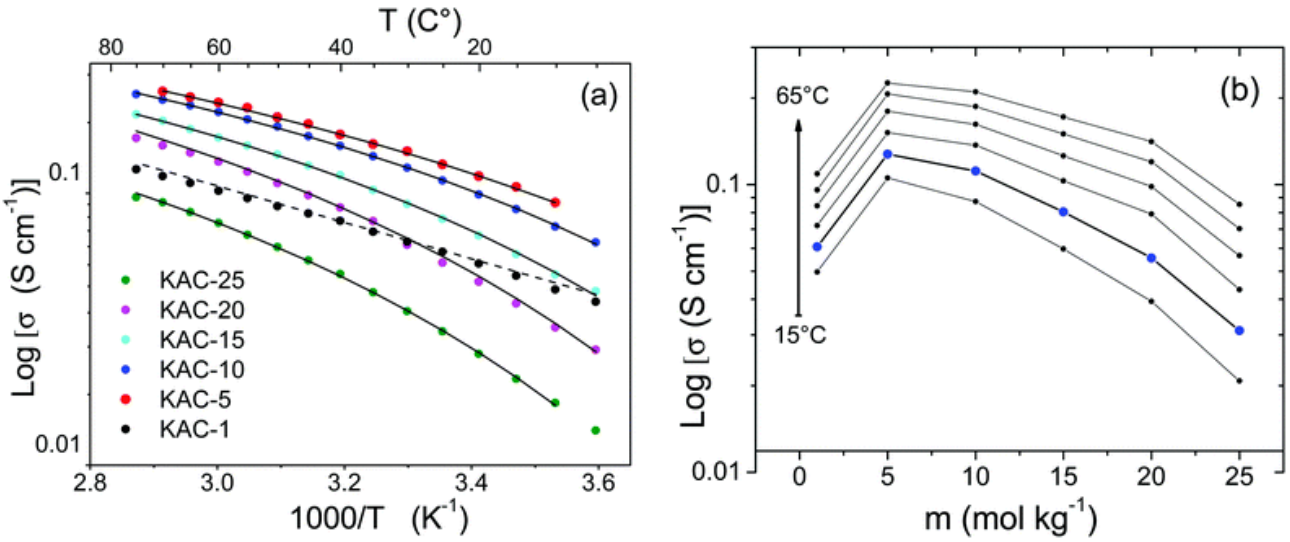

Fig. 3 (a) Arrhenius plot of the conductivity of KAC solutions. Continuous (-) and dashed (--) lines correspond to VTF and Arrhenius best-fits, respectively (R2 > 0.99); (b) isothermal conductivity vs.

solution molality at different temperatures ranging from 15 to 65 °C (ΔT = 10 °C). Blue dots represent the 25 °C conductivities.

The T_0 values increase with the concentration and are in reasonable agreement with the T_g values obtained from DSC measurements (see Fig. 1b), which shows a clear coupling between the ion transport and the diffusive particle motion which becomes significant above the glass transition temperature.[19] The behaviour of KAC-1 is anomalous and can be fitted by the Arrhenius equation similar to eqn (2) with a negative exponent. The best-fit gives an activation energy of 0.04 eV, in good agreement with the activation energy from viscosity (see Table 2).

The isothermal curves in Fig. 3b show a non-linear behaviour of the conductivity *vs.* concentration. At each temperature the curve maximum is observed for KAC-5, which at 25 °C (blue dots) has a conductivity of 128 mS cm^{-1}. However, the most concentrated solutions, KAC-20 and KAC-25, also show good conductivity values of 55.6 and 31.0 mS cm^{-1}, respectively. The KAC–water solutions follow the Kohlrausch law for strong electrolytes

$$\Lambda_m = \Lambda_0 - Ac^{1/2} \quad (4)$$

which calls for a linear dependence of Λ_m from the square root of the concentration (Fig. S7 in the ESI†). Here Λ_m and Λ_0 are the molar conductivity and the molar conductivity at infinite dilution, respectively, A is a constant, and c is the molarity of the solution. The Kohlrausch behavior calls for almost complete salt dissociation even at the highest attainable concentrations.

Given the availability of both conductivity and viscosity data, further information on the goodness of the KAC solutions as electrolytes can be obtained using the Walden relationship:[20]

$$\eta \propto \frac{1}{\Lambda_m} \quad (5)$$

which gives direct information on the ionicity of the system. Fig. 4 shows the Walden plot of the KAC solutions at different temperatures. As expected on the basis of the Kohlrausch behaviour, all the solutions behave as quasi-ideal electrolytes.

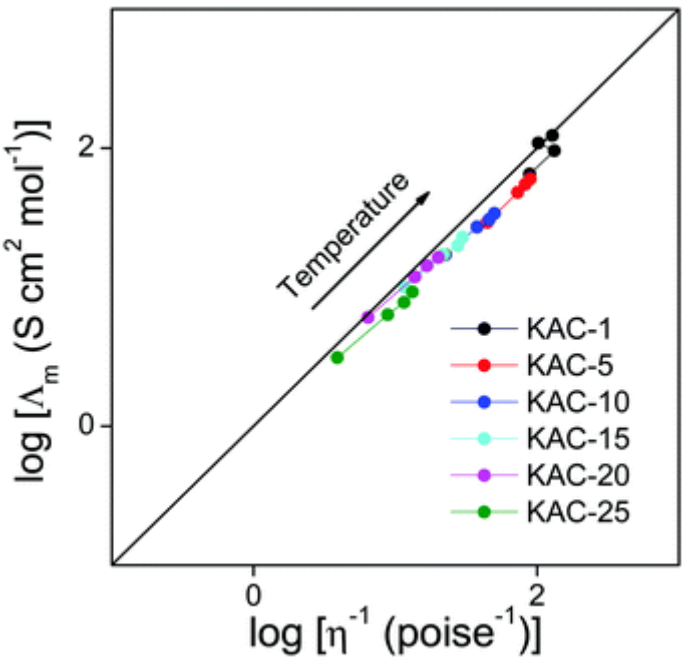

Fig. 4 *Walden plot of the KAC solutions at different temperatures. The full line shows the behaviour of aqueous KCl taken as the reference.*

The electrochemical stability windows of the solutions at different concentrations are presented in Fig. 5 in terms of anodic and cathodic decomposition potentials *vs.* the Standard Hydrogen Electrode (SHE), while the LSV current/potential profiles are shown in Fig. S8 in the ESI.† The KAC solutions have a pH that increases with the salt concentration (see the values in Table S1 in the ESI†) and this causes a variation in the thermodynamic values of anodic and cathodic decomposition potentials of water which are shown as solid lines in the figure. The anodic branch of the curves shows that all samples are relatively stable and the addition of salt does not change the value. This is the effect of two contrasting aspects: the salt addition decreases the activity coefficient of water and therefore increases the stability, which is however also influenced by the increase in pH which tends to lower the decomposition limit. In the case of the cathodic scans, instead, the negative decomposition limit monotonically increases with concentration and this increase is greater than expected considering only the pH effect. Water-in-salt solutions (>15 m) have thus lower decomposition potentials, thanks to the distinct interaction of water with the ions, as widely described in the Raman section, which probably reduces the activity coefficient of water. KAC-20 and KAC-25 show, indeed, the best stabilities: the former is stable up to ≈−1.19 *vs.* SHE while the latter is stable up to −1.24 *vs.* SHE.

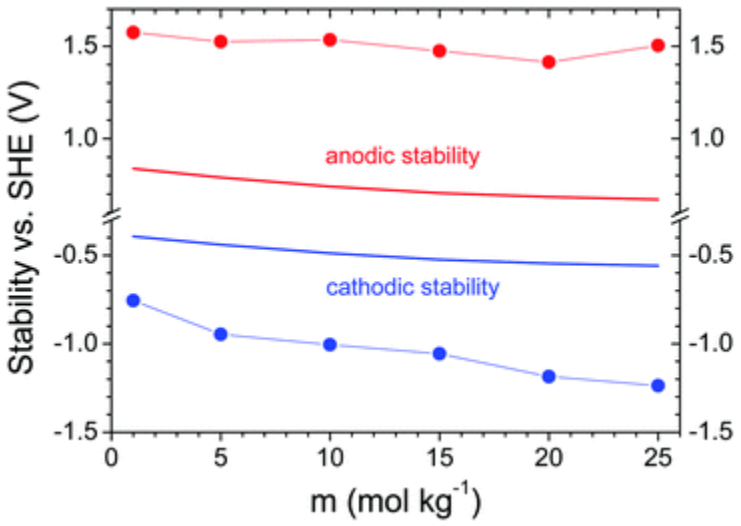

Fig. 5 Cathodic (blue dots) and anodic (red dots) decomposition limits vs. SHE for different solutions. The blue and red full lines indicate the thermodynamic limits of water in oxidation and reduction, respectively, as calculated from the Nernst law at different pH values.

The electrochemical stability windows of KAC-20 and KAC-25 become 2.6 and 2.7 V wide, respectively, which are much larger than those of aqueous solutions currently used in supercapacitors and even greater than that of the same system tested by Pan *et al.*[9] Interestingly, Pan *et al.* obtained a narrower value but observed an enhanced stability not only on the cathodic but also the anodic side, and this difference is most probably due to the choice of working electrodes.

A representative Raman spectrum of the investigated set is shown in Fig. 6. The spectrum shows all the main vibrational modes expected for the potassium acetate–water system, as already reported in the literature.[21–23] In particular, from low to high wavenumbers the main Raman features are ascribed to COO rocking and deformation (in the range below 750 cm^{-1}), C–C stretching (a strong peak at 925 cm^{-1}), CH_3 deformation (a sharp peak at 1344 cm^{-1}), CO stretching (a peak at 1413 cm^{-1}), CH stretching (two peaks at about 3000 cm^{-1}), and water related stretching bands (broad peaks in the range above 3000 cm^{-1}). For a detailed list of the observed peaks and their interpretation see Table S2 in the ESI.† To extract useful information about the aggregation of KAC molecules in the binary mixture, we focused our attention on the CO stretching peak. Indeed, this mode can be adopted as a sensitive probe of the COO^- interaction with the surrounding species: water molecules, K^+ cations, and the other CH_3COO^- anions. To perform a reliable comparison between the different KAC solutions, we used the CC stretching mode as an internal reference peak for an accurate analysis of peak positions. In fact, we suppose that the CC

skeleton is not affected by the acetate concentration which, in turn, is expected to alter mainly the COO^- vibrational modes. Thus, the spectra were appropriately shifted so as to fix the position of the CC stretching exactly at 925 cm^{-1}. The CO stretching bands, after baseline correction and normalization, are shown in Fig. 7. Peak broadening and shifting towards higher wavenumbers was observed with the KAC concentration increase.

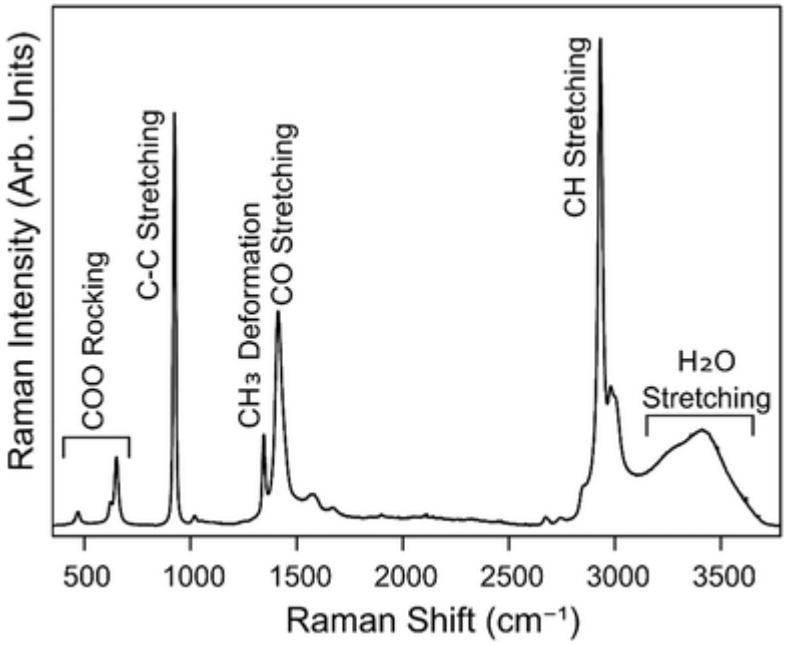

Fig. 6 *Representative Raman spectrum of KAC-25.*

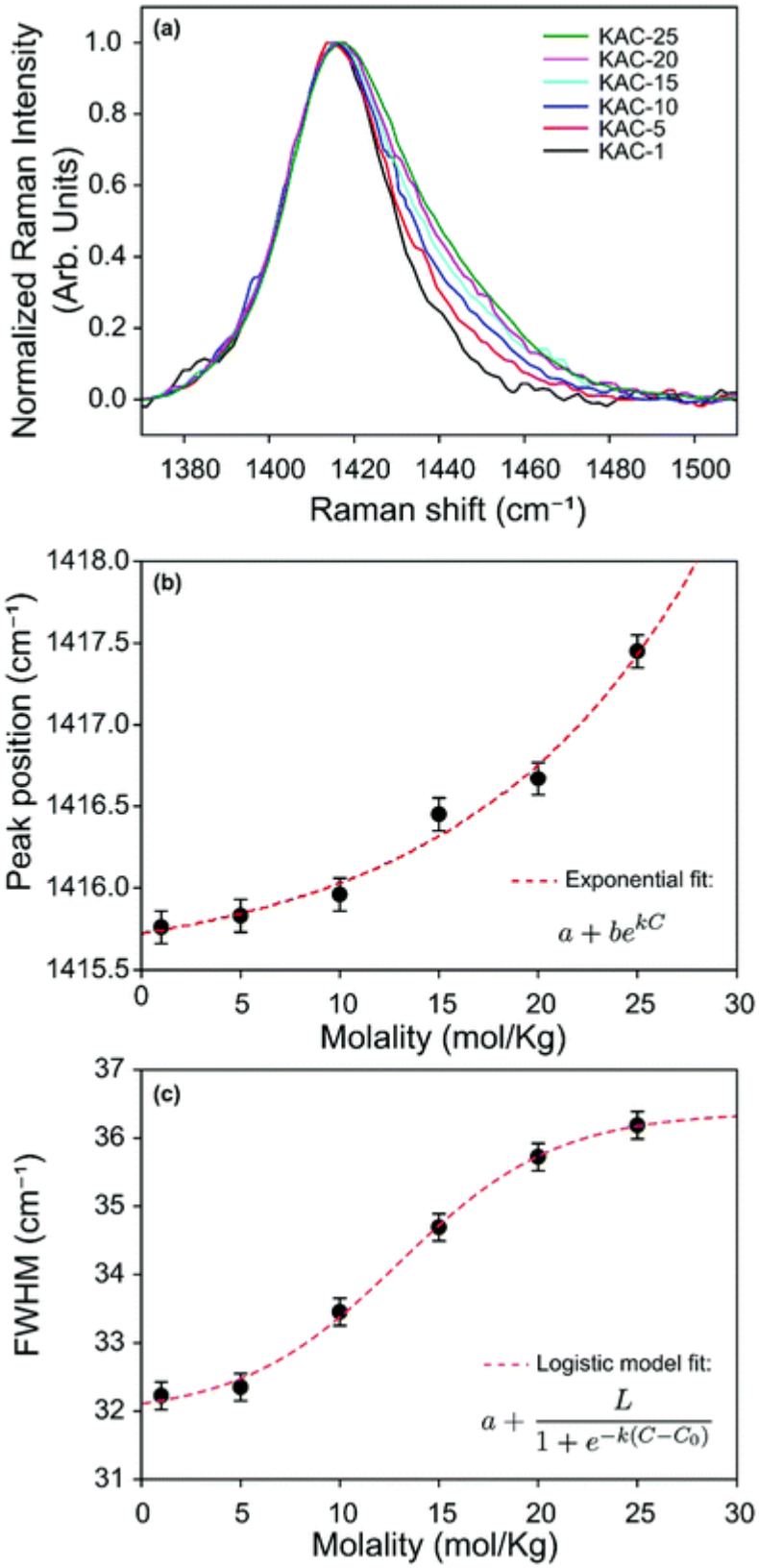

Fig. 7 *The CO stretching signal at different KAC concentrations (a) and the peak position (b) and FWHM of the peak (c) vs. the salt molality.*

Specifically, the peak appears to be a result of the superposition of at least two peaks. These peaks have been fitted using a sum of Voigt profiles; however, the fitting results are not satisfactory since the system may converge to many different results, all with acceptable residues. Thus, we prefer not to stress the quantitative results of such fittings, but to analyse directly the measured position and the measured Full Width at Half Maximum (FWHM) of the peak as summarized in Fig. 7b and c, respectively. The position of the maximum as a function of the KAC content follows an exponential law, shifting from 1415.8 cm^{-1} to 1417.5 cm^{-1} when passing from sample KAC-1 to KAC-25. In the framework of a simple harmonic oscillator, this shift clearly indicates a strengthening of the CO bond as the concentration of the acetate ions increases. The effect of intermolecular interactions on the vibrational spectra is even more pronounced if we assume apparent FWHM as a function of KAC concentration. In this case we register peak broadening that follows a simple sigmoidal function. To approximate the observed behaviour we tentatively fitted the data by a logistic model:

$$a + \frac{L}{1 + e^{-k(C - C_0)}} \quad (6)$$

where a (= 31.94 cm^{-1}, from fitting) is an offset value of the FWHM observed at a low concentration, L (= 4.44 cm^{-1}) is the limit value of the FWHM increment at a high concentration, k (0.25 kg mol^{-1}) is the growth rate, C is the KAC molality and C_0 (13.0 mol kg^{-1}) is the midpoint of the sigmoid function and represents the concentration at which the COO^- vibrational mode changes between two configurations (see also Table S3 in the ESI†).

Interestingly, the fitted value of C_0 corresponds to 4.3 molecules of water per acetate molecule, and thus for $C < C_0$ the COO^- environment is prevalently made of water molecules and responds as a fully hydrated anion and for $C > C_0$ the COO^- vibration is locally modified by the presence of species other than water molecules. This number is in accordance with the reported value of the hydration number in the first hydration shell of acetate salts, which lies between 4.5 and 7, according to experimental[24,25] and computational results.[26,27]

Hence, the observed behaviour of the inhomogeneous broadening is related to a change in the availability of water molecules interacting with K^+ ions, in excellent agreement with viscosity and conductivity data.

For the highest KAC concentrations, the number of water molecules is no longer able to properly shell cations, and the COO^- moiety starts to interact with them, although without

producing significant ion reassociation, leading to the modification of hydrogen bonding which affects the position and FWHM of the CO stretching.[28]

Conclusions

In this paper we have reported a thorough physico-chemical characterization study of KAC–H_2O solutions which are of interest for most electrochemical applications, including energy storage. The thermal (DSC) and spectroscopic (Raman) analyses demonstrated that there is a concentration threshold between 10 and 15 in molality which changes the physico-chemical characteristics of the KAC solutions. Across the entire compositional range, the KAC solutions behave as strong electrolytes, as demonstrated by the Kohlrausch behaviour. However, below 10–15 mol kg^{-1} all the ions are fully hydrated and long-range ion–ion interactions affect the electrical conductivity. Above the limit of 15 mol kg^{-1}, the water molecules are not enough to fully screen ion–ion interactions, which affect both the ionic transport properties and the thermal behaviour of the solutions, the T_g values of which now increase with the salt concentration. This may be interpreted as a transition between "salt-in-solvent" and "solvent-in-salt" regimes. The cathodic decomposition potential decreases to 350 and 400 mV for KAC-25 and KAC-20, respectively, compared to KAC-1, thanks to the reduced activity of water at a high concentration. The electrochemical stability windows of the concentrated solutions are thus increased to about 2.5 V. This value, together with a conductivity higher than 30 mS cm^{-1} at room temperature, may enable the use of KAC-20 and KAC-25 in water-based K-ion batteries or even in high-energy supercapacitors, which can take full advantage of this larger potential window.

Authors contribution

P. L. S. and N. P. led the investigations and the data curation; S. B., M. M., B. V., and R. L. contributed to investigations and the data curation; R. R. and P. M. led the conceptualization and the methodology and supervised the investigations; R. S., V. B., S. R., and R. L. contributed to the methodology; R. R. and P. M. led the writing; P. L. S. and R. L. contributed to the writing; and all authors contributed equally to the review and editing of the manuscript.

Conflicts of interest

There are no conflicts to declare.

Acknowledgements

This work has been financially supported by the Ministry of University and Research (MIUR) through grant “Dipartimenti di Eccellenza – 2017 Materials for Energy”.

References

1 R. M. Fuoss and F. Accascina, Electrolytic Conductance, Interscience Publishers, New York, 1959.

2 J. E. Desnoyers and C. Jolicoeur, Comprehensive Treatise of Electrochemistry: Thermodynamics and Transport Properties of Aqueous and Molten Electrolytes, Springer, New York, 1st edn, 1983, ch. 1–2, vol. 5.

3 J. C. Justice, Comprehensive Treatise of Electrochemistry: Thermodynamics and Transport Properties of Aqueous and Molten Electrolytes, Springer, New York, 1st edn, 1983, ch. 3, vol. 5.

4 K. Xu, Chem. Rev., 2004, 104(10), 4303–4418.

5 L. Suo, Y. S. Hu, H. Li, M. Armand and L. Chen, Nat. Commun., 2013, 4(1), 1–9.

6 C. A. Angell, C. Liu and E. Sanchez, Nature, 1993, 362(6416), 137–139.

7 W. Chen, Y. Wu, Y. Yue, J. Liu, W. Zhang and X. Yang, et al., Science, 2015, 350(6263), 944–948.

8 X. Zang, C. Shen, E. Kao, R. Warren, R. Zhang and K. S. Teh, et al., Adv. Mater., 2018, 30, 1704754.

9 Z. Tian, W. Deng, X. Wang, C. Liu, C. Li and J. Chen, et al., Funct. Mater. Lett., 2017, 10(06), 1750081.

10 D. P. Leonard, Z. Wei, G. Chen, F. Du and X. Ji, ACS Energy Lett., 2018, 3(2), 373–374.

11 M. R. Lukatskaya, J. I. Feldblyum, D. G. Mackanic, F. Lissel, D. L. Michels and Y. Cui, et al., Energy Environ. Sci., 2018, 11(10), 2876–2883.

12 H. Feuer, A. Seidell and W. F. Linke, Solubilities of Inorganic and Organic Compounds: A Compilation of Solubility Data from the Periodical Literature, Supplement to edn 3, Van Nostrand, New York, 1952.

13 P. Mustarelli, C. Tomasi and A. Magistris, Z. Naturforsch., 1996, 51(3), 187–191.

14 R. Bouaziz and J.-Y. Basset, Compt. Rend., 1966, 263(8), 581–584.

15 Z. Dobrokhotova, S. Yashchenko, Y. Nadtochii, S. Zakharov, E. Kubyshkina and Y. Berezovskaya, Zh. Fiz. Khim., 1992, 66(5), 1426–1429.

16 S. Tanaka, K. Ogawa and N. Sasaki, Netsu Bussei, 2015, 29(3), 129–134.

17 D. S. Viswanath and G. Natavajan, Data book on the viscosity of liquids, Hemisphere Publishing, New York, NY, USA, 1989.

18 X. Wu, S. Xu, D. Wu and H. Liu, Chin. J. Chem. Eng., 2018, 26(12), 2581–2591.

19 P. Mustarelli, C. Capiglia, E. Quartarone, C. Tomasi, P. Ferloni and L. Linati, Phys. Rev. B: Condens. Matter Mater. Phys., 1999, 60(10), 7228–7233.

20 C. A. Angell, Y. Ansari and Z. Zhao, Faraday Discuss., 2011, 154(0), 9–27.

21 I. Durickovic, in Applications of Molecular Spectroscopy to Current Research in the Chemical and Biological Sciences, ed. M. T. Stauffer, InTech, 2016, DOI: 10.5772/64550.

22 W. Rudolph and G. Irmer, RSC Adv., 2015, 5(28), 21897–21908.

23 K. Ito and H. J. Bernstein, Can. J. Chem., 1956, 34(2), 170–178.

24 M. V. Fedotova and S. E. Kruchinin, J. Mol. Liq., 2011, 164(3), 201–206.

25 H. Naganuma, Y. Kameda and T. Usuki, J. Phys. Soc. Jpn., 2001, 70, 356–358.

26 T. Liang and T. R. Walsh, Phys. Chem. Chem. Phys., 2006,8(38), 4410–4419.

27 A. Payaka, A. Tongraar and B. M. Rode, J. Phys. Chem. A, 2009, 113(13), 3291–3298.

28 K. Tanabe, J. Raman Spectrosc., 1984, 15(4), 248–251